Aerosol-cloud interactions in mixed-phase convective clouds. Part 1: Aerosol perturbations.
Supplementary Information

Annette K. Miltenberger[1], Paul R. Field[1,2], Adrian A. Hill[2], Phil Rosenberg[1], Ben J. Shipway[2], Jonathan M. Wilkinson[2], Robert Scovell[2], and Alan M. Blyth[3]

[1]Institute of Climate and Atmospheric Science, School of Earth and Environment, University of Leeds, United Kingdom
[2]Met Office, Exeter, United Kingdom
[3]National Centre for Atmospheric Science, School of Earth and Environment, University of Leeds, United Kingdom

Correspondence to: Annette K. Miltenberger (a.miltenberger@leeds.ac.uk)
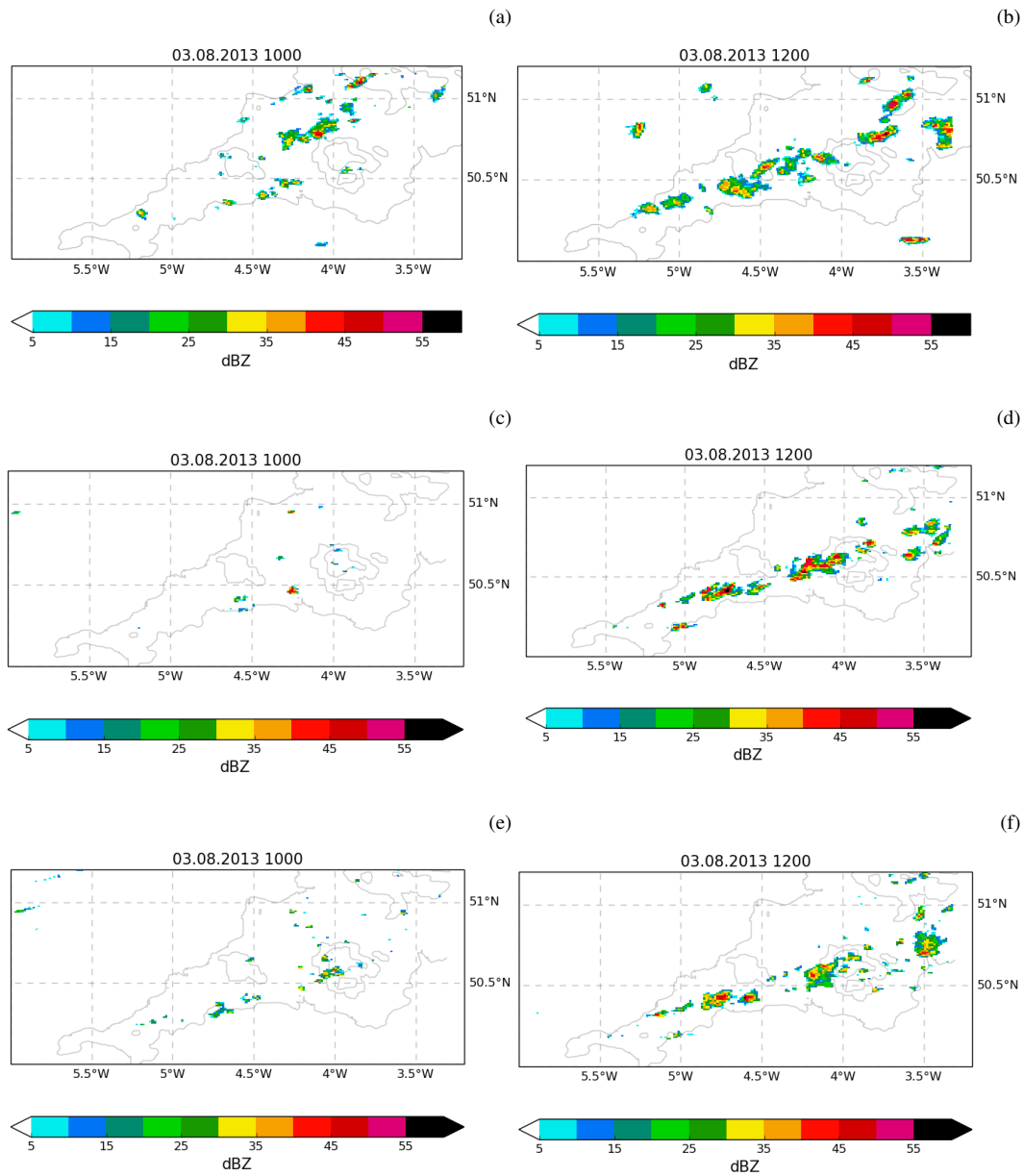
Figure 1. Column maximum radar reflectivity over the COPE domain at 10 UTC (a,c,e) and 12 UTC (b,d,f) from the operational radar network (a,b), the model simulations with passive aerosol (c,d) and with aerosol processing (e,f).
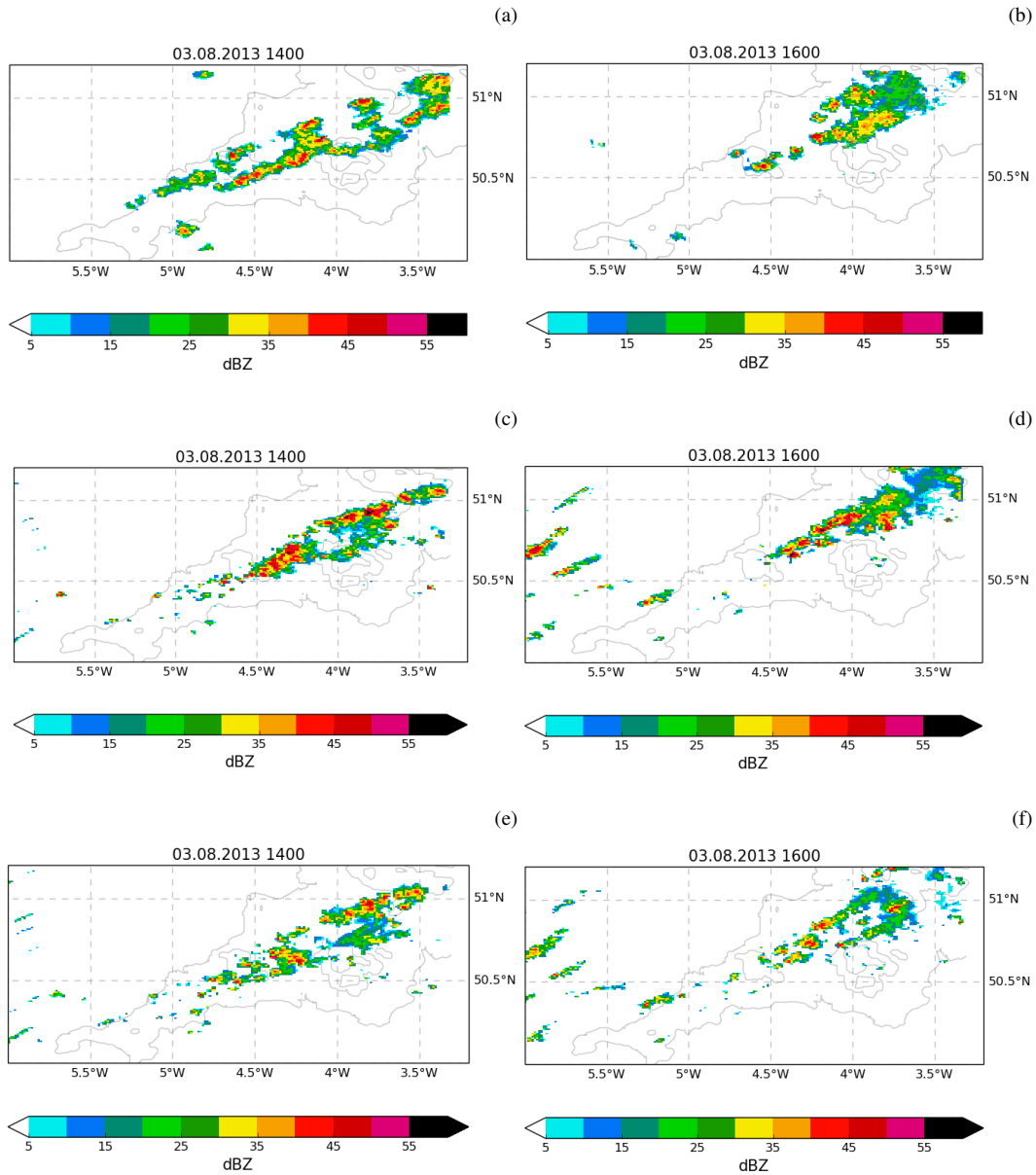
Figure 2. Column maximum radar reflectivity over the COPE domain at 14 UTC (a,c,e) and 16 UTC (b,d,f) from the operational radar network (a,b), the model simulations with passive aerosol (c,d) and with aerosol processing (e,f).
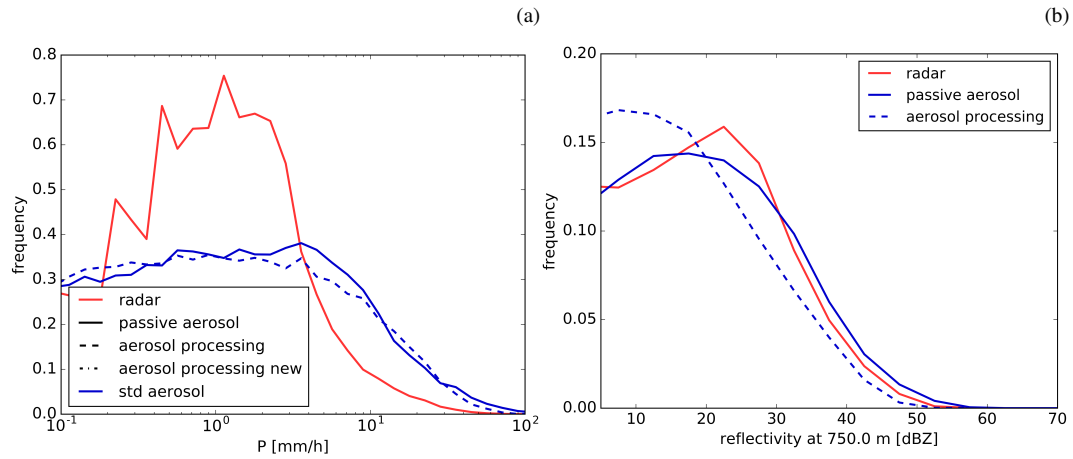
Figure 3. Comparison of the distribution of (a) surface precipitation rate and (b) radar reflectivity at 750 m from model simulations with the standard aerosol profile (blue) and radar observations (red). The solid line shows results from the simulation with passive aerosols and the dashed line from the simulation with aerosol processing. Simulated precipitation rates and radar reflectivity have been coarse-grained to the spatial resolution of the radar observations (1 km horizontal and 500 m vertical).
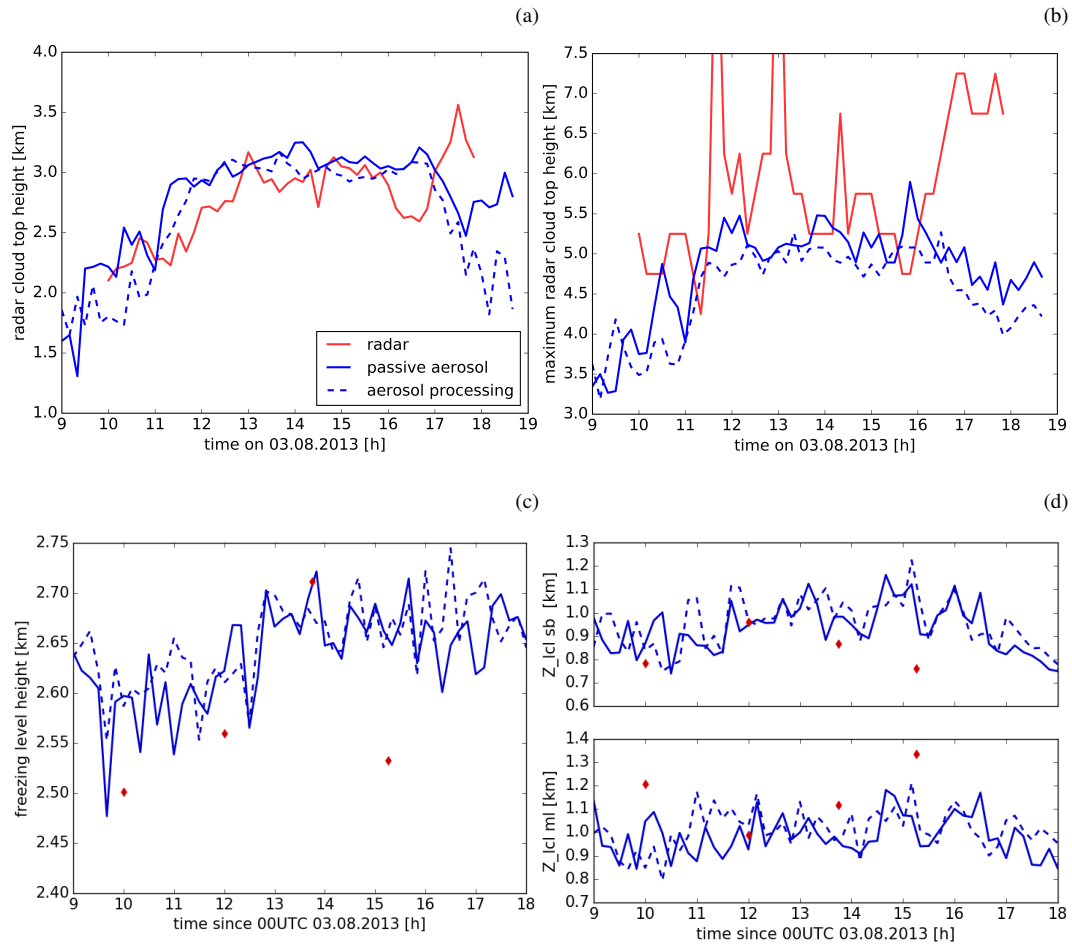
Figure 4. Comparison of domain mean (a) and maximum (b) radar cloud top height from the model simulation against radar data. Cloud top height is defined as the highest altitude at which the radar reflectivity reaches $18\,\mathrm{dBZ}$. Timeseries of $0\,^{\circ}\mathrm{C}$ level height (c) and lifting condensation level (d) from the radiosondings at Davidstow (red diamonds) and the closest model gridpoint (blue lines).
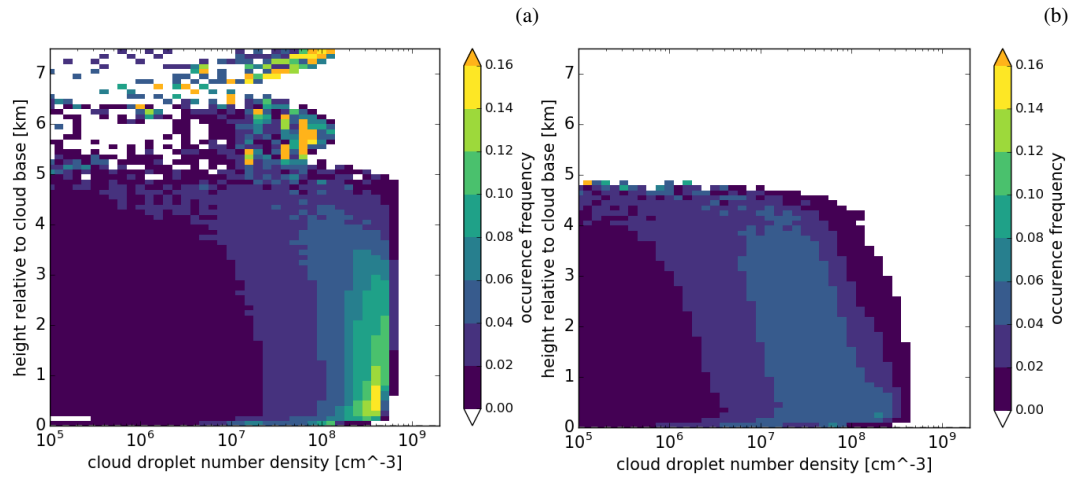
Figure 5. Cloud droplet number concentration from simulations with passive aerosol (a) and aerosol processing (b) as a function of altitude above cloud base. Cloud base is defined as the lowest model level in each column with a cloud droplet mass larger than $1 \, \mathrm{g kg^{-1}}$.

(a) (b)
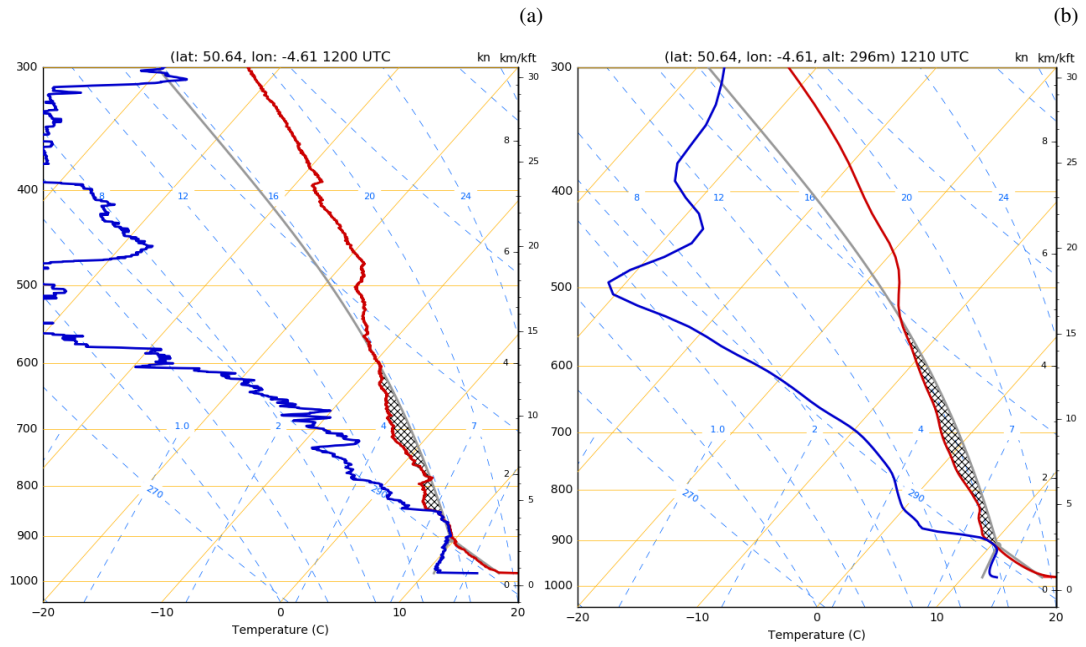
Figure 6. Thermodynamic profiles from radiosonde released at Davidstow at 1200 UTC (a) and from the closest grid point in the model (b).
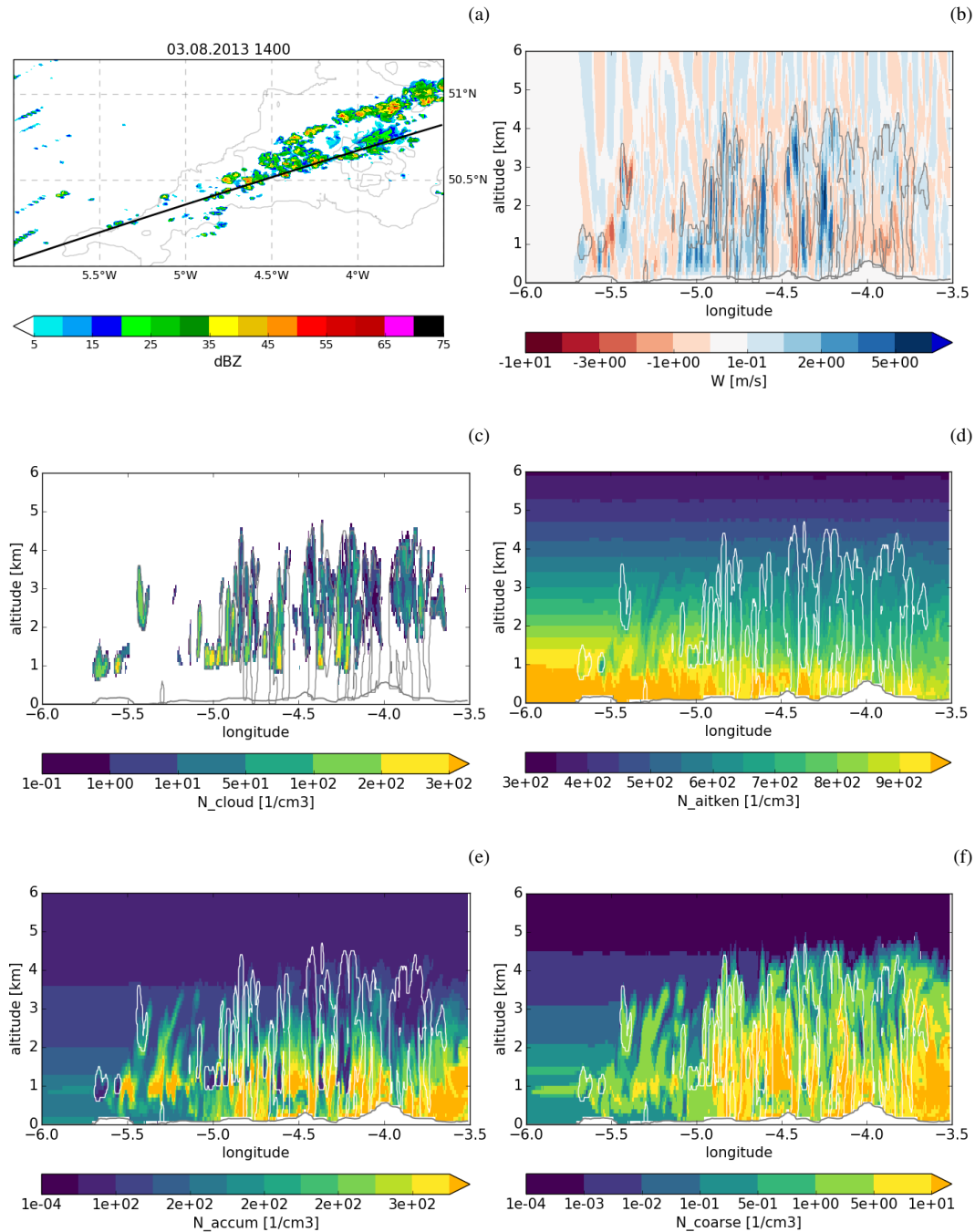
Figure 7. Aerosol fields from the simulation with aerosol processing at 14 UTC. (a) Colour shading shows the column maximum reflectivity and the black line indicates the location of the cross-sections plotted in the other panels: (b) Vertical velocity with blueish colours indicating regions of updraft and redish colours regions of downdrafts. Number densities of cloud droplets (c), Aitken mode aerosol (d), accumulation mode aerosol (e) and coarse mode aerosol (f). The contour lines (grey in panel b & c, white in panels d-f) indicate areas with hydrometeor mixing ratios larger than 10^{-3} gkg^{-1}.

8
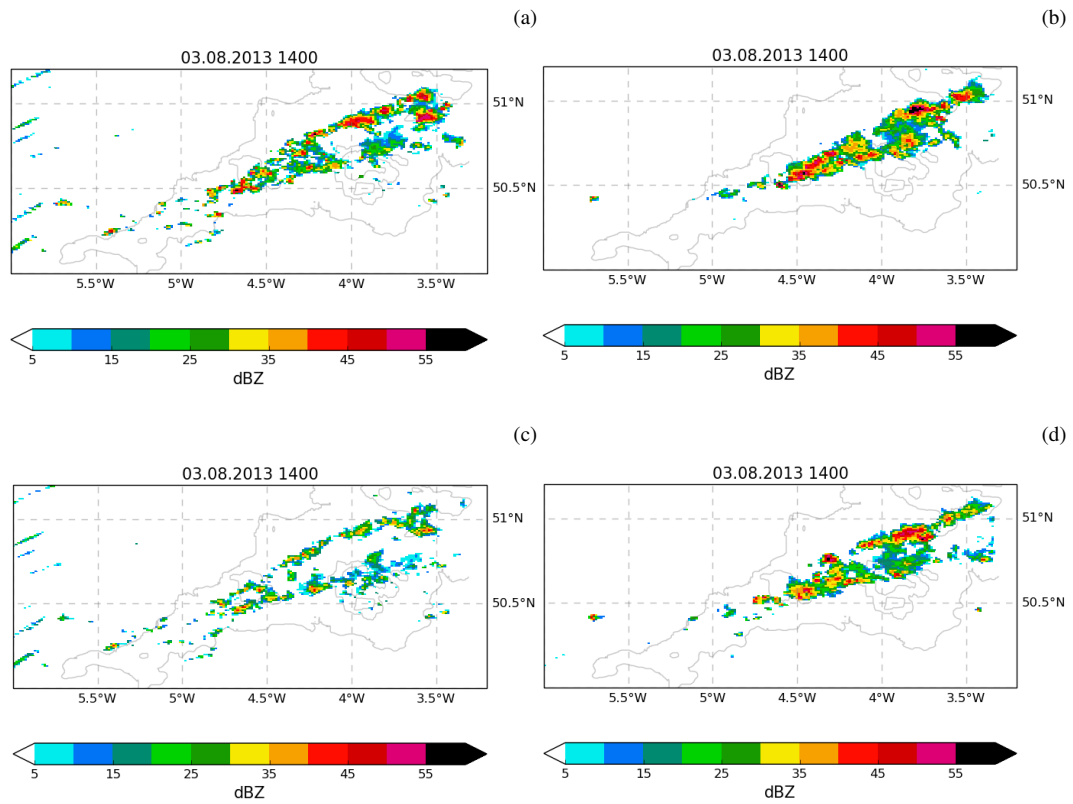
Figure 8. Column maximum radar reflectivity over the COPE domain at 14 UTC from the simulations with passive aerosol (a,b) and with aerosol processing (c,d). The left panels are from simulations with the lower aerosol concentrations and the right panels from those with higher aerosol concentrations.
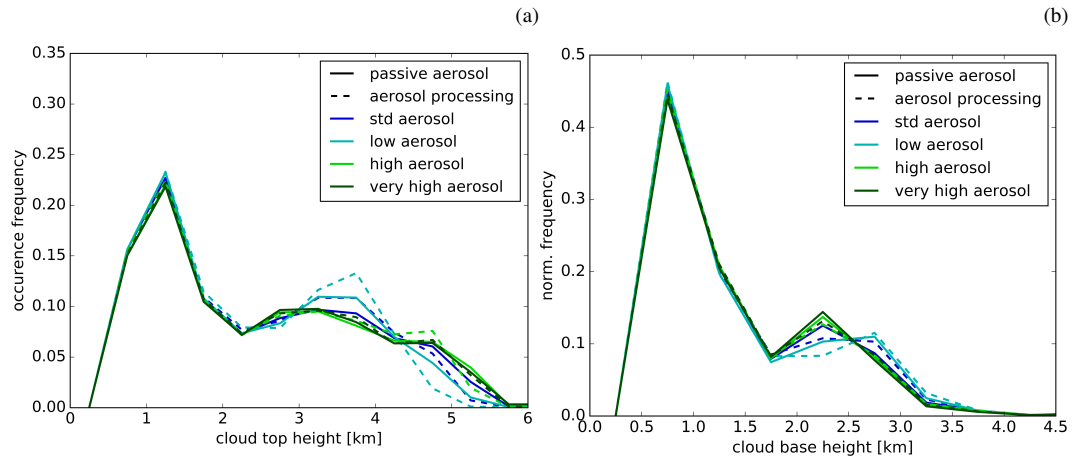
Figure 9. Distribution of cloud top (a) and cloud base height (b) in the different simulations. Cloud top (base) is defined as the highest (lowest) point in each column where the sum of cloud and ice water content exceeds $1\ \mathrm{mgkg}^{-1}$.
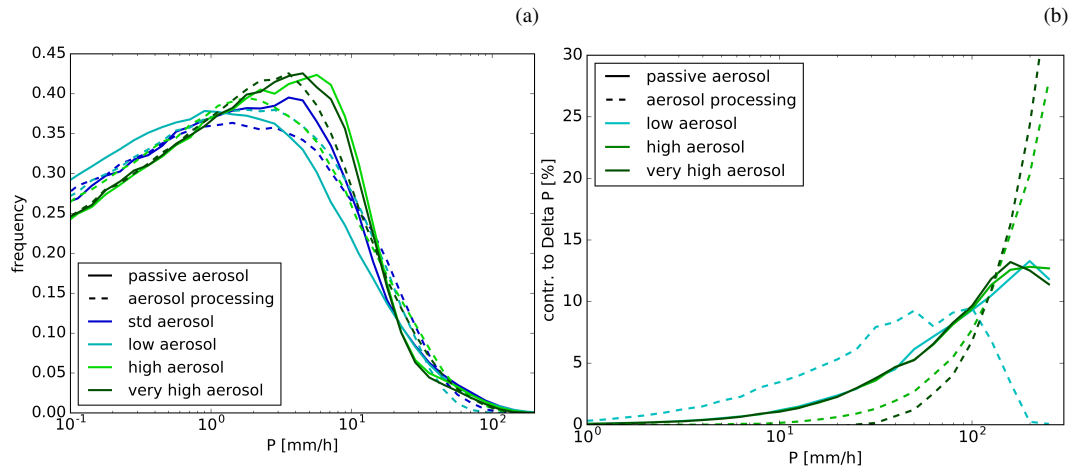
Figure 10. The precipitation rate distribution between 9 UTC and 21 UTC (a) and the contribution of specific precipitation rates to the change in domain accumulated precipitation (b). Different line colours indicate the different aerosol initial conditions, solid lines correspond to simulations with passive aerosols and dashed lines to simulations with aerosol processing.
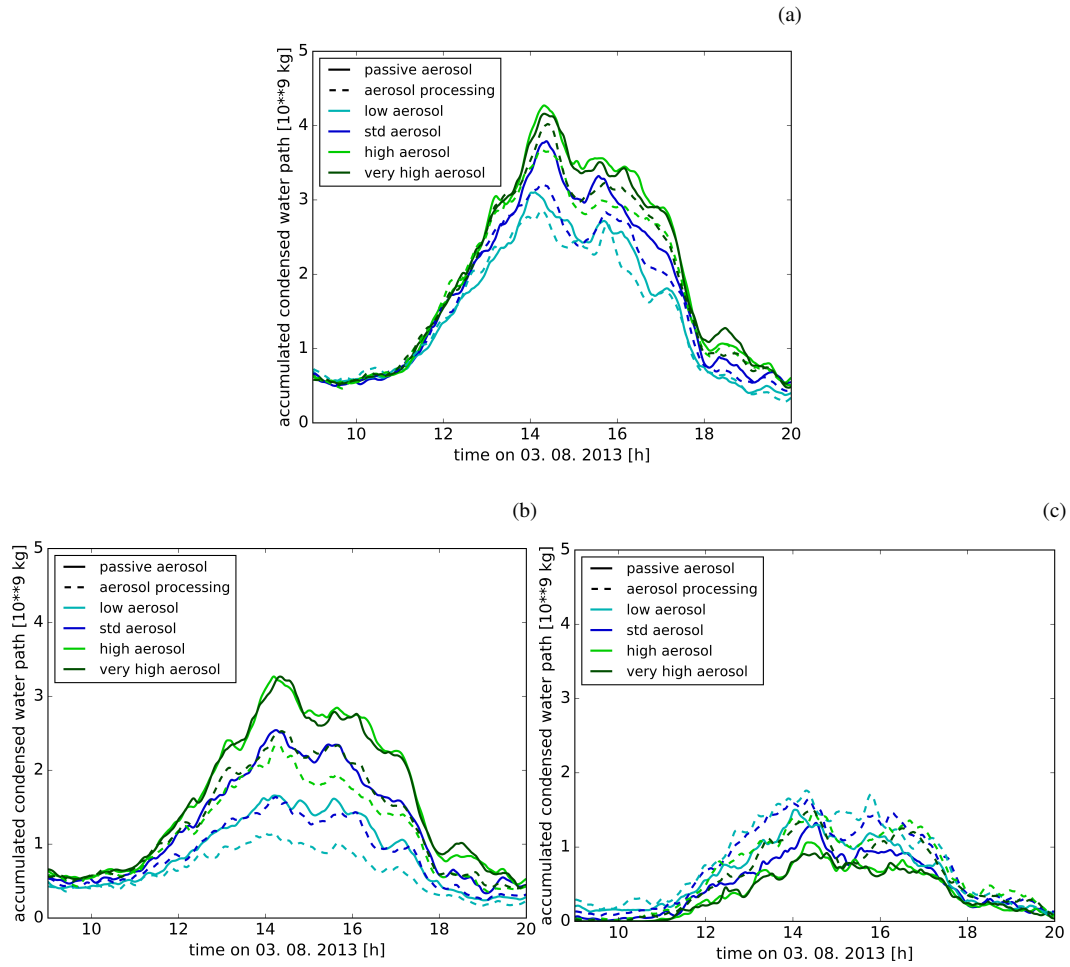
Figure 11. Time evolution of condensed water path in (c) all hydrometeor categories, (b) the cloud, ice and snow categories, and (c) the graupel and rain categories. Different line colours indicate the different aerosol initial conditions, solid lines correspond to simulations with passive aerosols and dashed lines to simulations with aerosol processing.
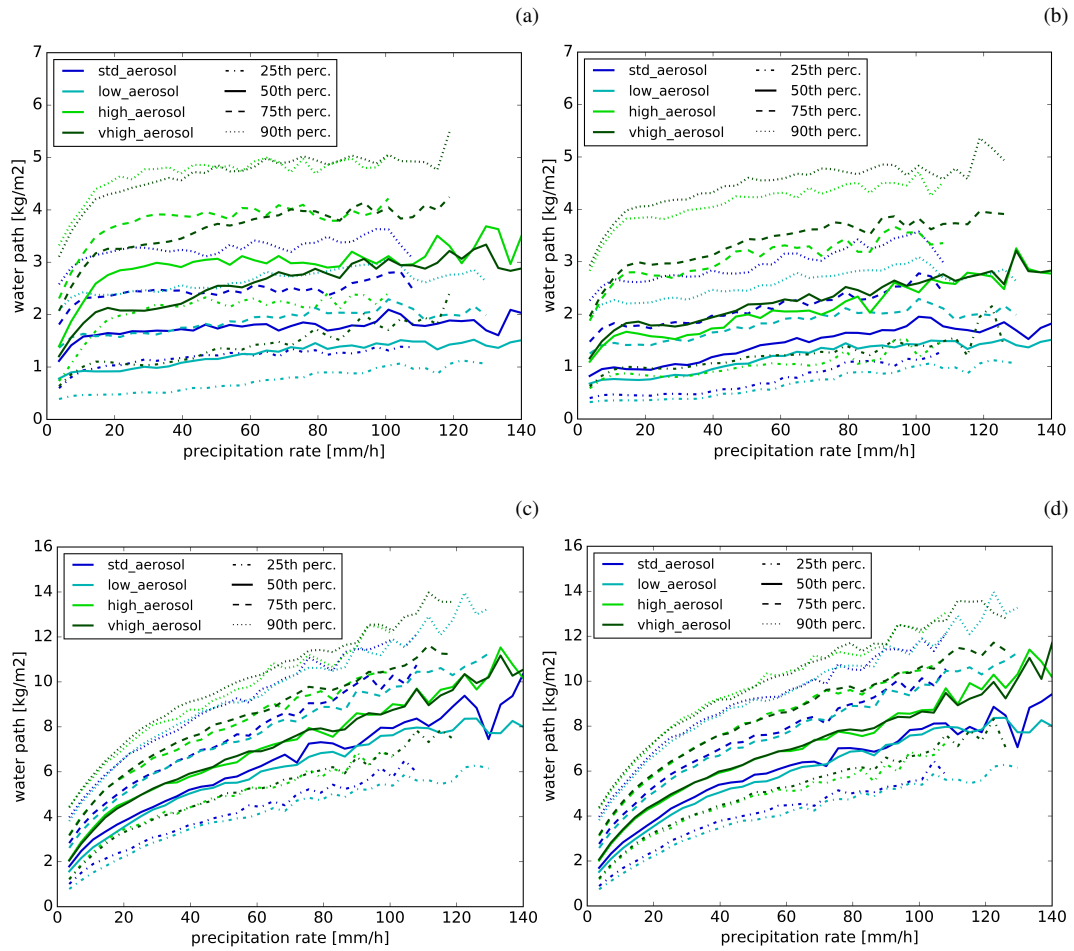
**Figure 12.** Percentiles of condensed water path (*top:* including ice, snow and cloud droplet species, *bottom:* all hydrometeors) in columns with certain precipitation rate. The *left* panels show simulations with passive aerosols and the *right* panels those with aerosol processing. Different colours correspond to the different aerosol profiles and different line styles to the different percentiles
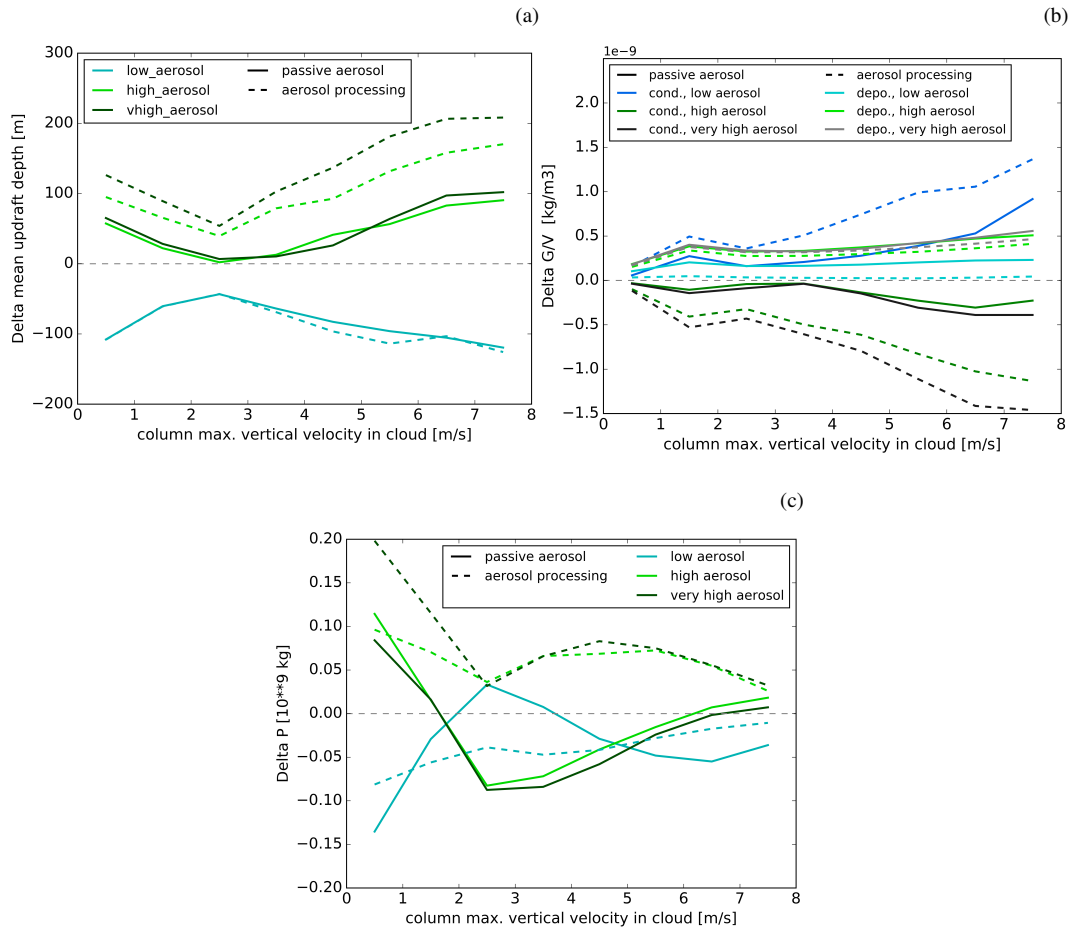
Figure 13. (a) Mean depth of updraft regions ($w > 0\ \mathrm{ms}^{-1}$ and $q > 1\ mgkg^{-1}$) classified by maximum column in-cloud vertical velocity. (b) Change mean condensation, evaporation, deposition and sublimation rates for each maximum in-cloud vertical velocity bin. (c) Change in accumulated precipitation from each w_{max} bin. Results from simulations with higher (lower) aerosol loading are depicted in green (blue). Solid lines correspond to simulations with passive aerosol, dashed lines to simulations with aerosol processing.
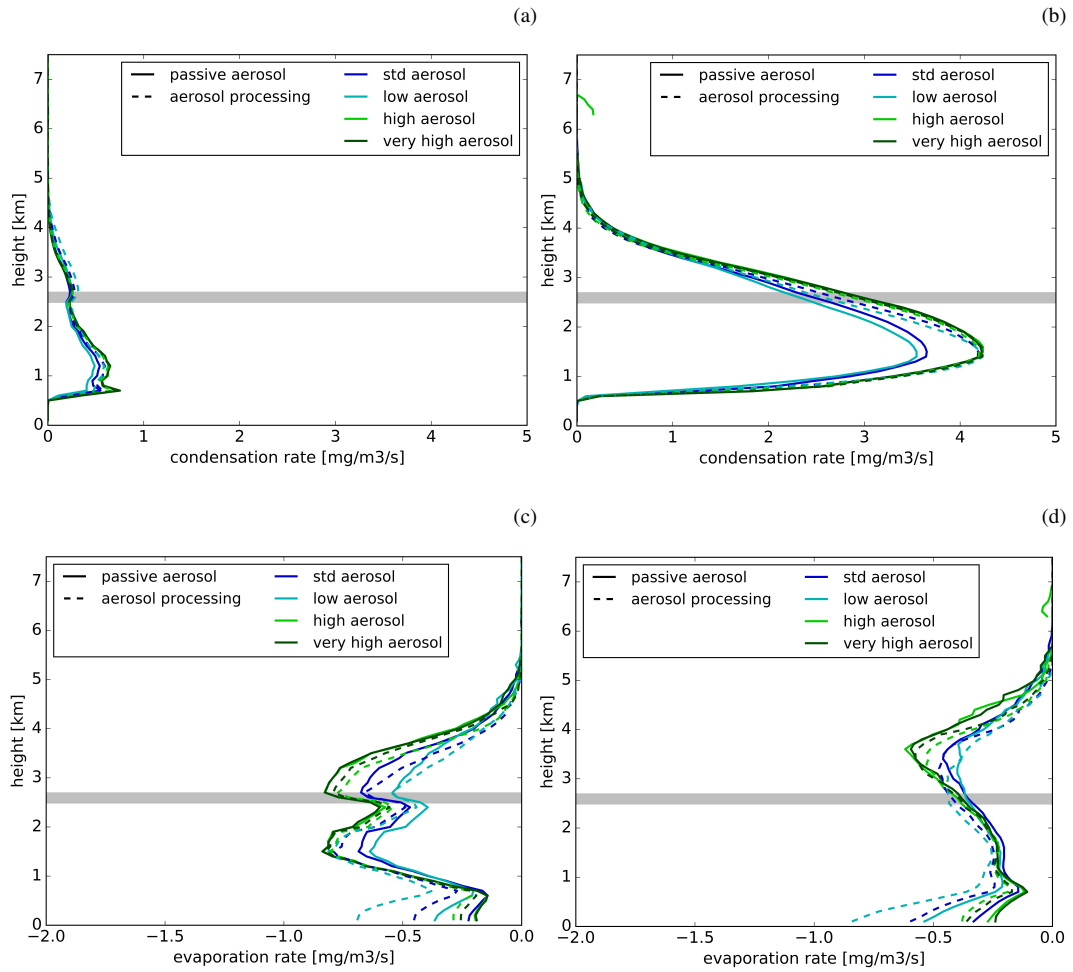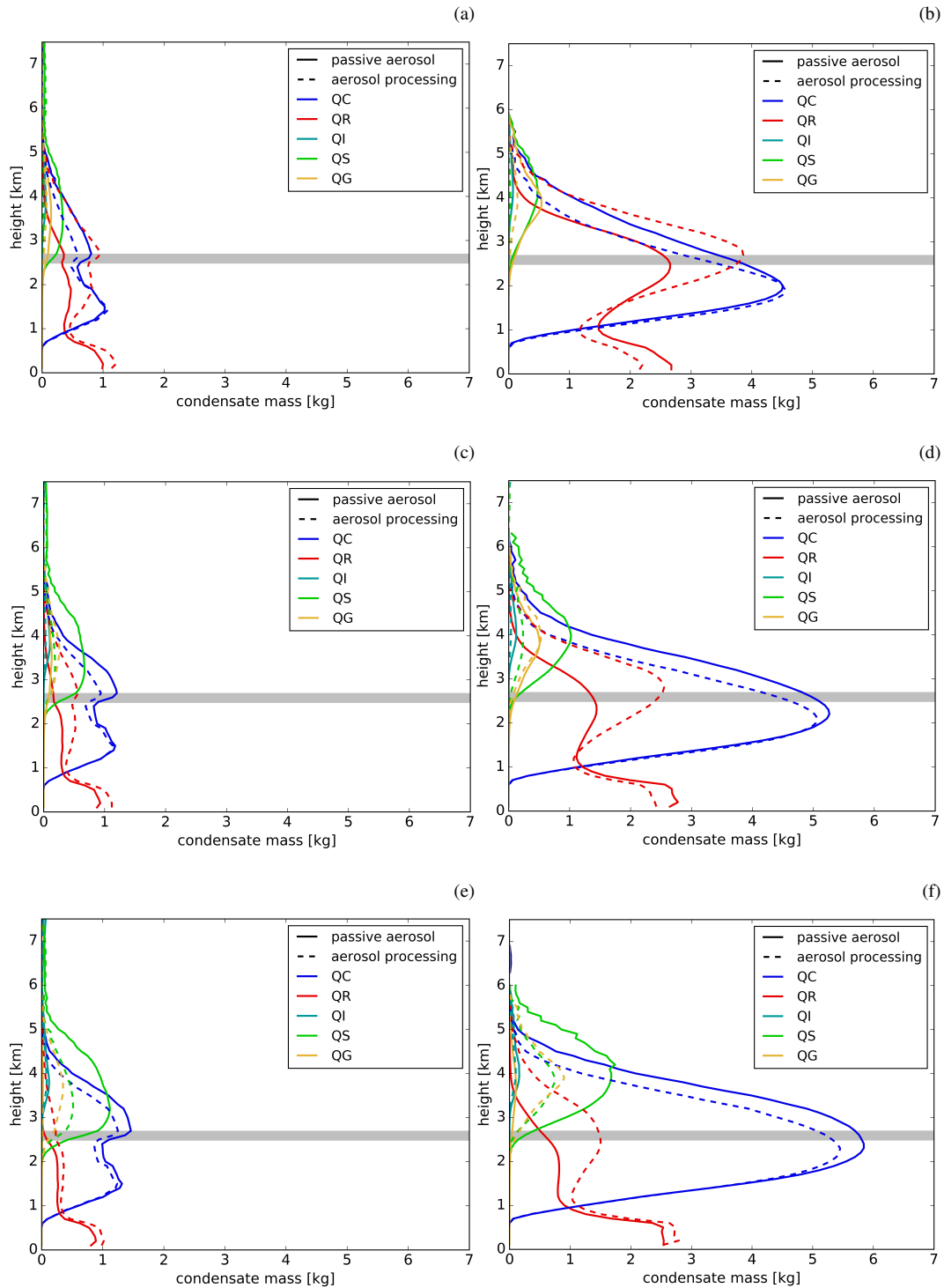
Figure 14. Average profiles of condensation (a,b) and evaporation (c,d) rates. The left panels shows the average over all columns with a column maximum vertical velocity of $0 - 3\,\mathrm{ms}^{-1}$ and the right panels for those with a column maximum vertical velocity larger than $3\,\mathrm{ms}^{-1}$. The grey horizontal line indicates the location of the $0\,^{\circ}\mathrm{C}$ line in the different simulations.
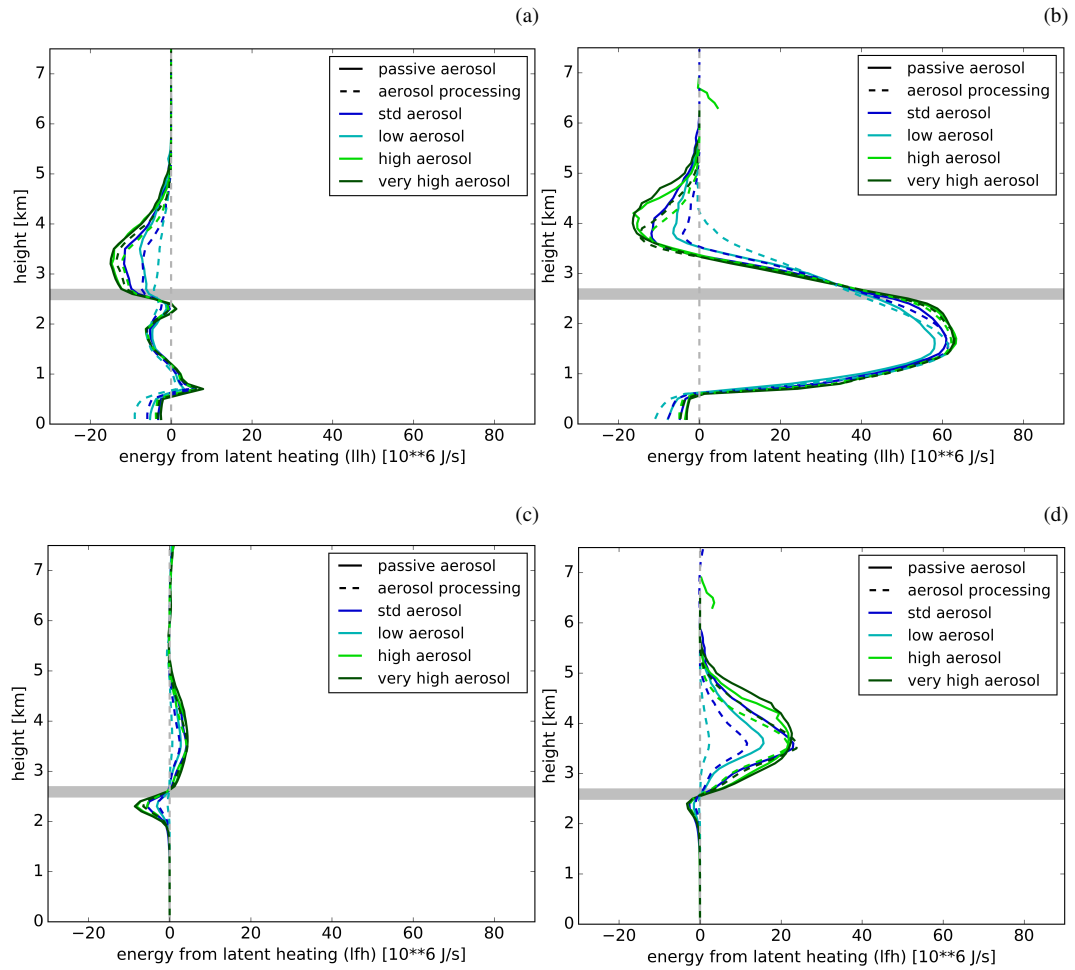
Figure 15. Average profiles of latent heat release by changes in liquid (a, b) and solid (c, d) cloud condensate. The left panels shows the average over all columns with a column maximum vertical velocity of $0 - 3\,\mathrm{ms}^{-1}$ and the right panels for those with a column maximum vertical velocity larger than $3\,\mathrm{ms}^{-1}$. The grey horizontal line indicates the location of the $0\,^{\circ}\mathrm{C}$ line in the different simulations.

Figure 16. Average profiles of mean mixing ratio of the different hydrometeors (colours) for simulations with low (a, b), standard (c, d) and high (e, f) aerosol concentrations. The left panels shows the average over all columns with a column maximum vertical velocity of $0 - 3 \, \mathrm{m s}^{-1}$ and the right panels for those with a column maximum vertical velocity larger than $3 \, \mathrm{m s}^{-1}$. Solid lines represent simulations with passive aerosols and dashed lines those with aerosol processing. The grey horizontal line indicates the location of the $0 \, ^{\circ}\mathrm{C}$ line in the different simulations.
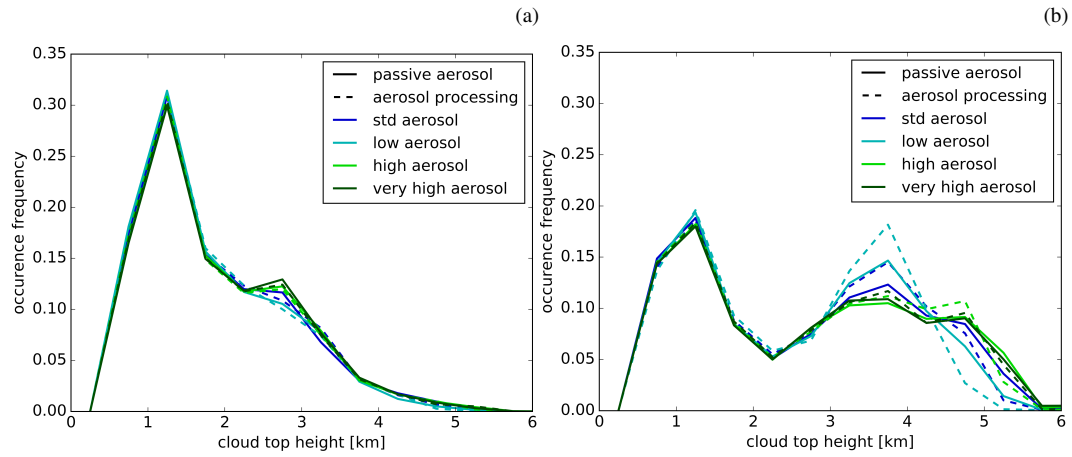
Figure 17. Distribution of cloud top height in the different simulations for the time period between 9 UTC to 12 UTC (a) and 12 UTC to 19 UTC (b), respectively. Cloud top is defined as the highest point in each column where the condensate content exceeds $1 \, \mathrm{mgkg}^{-1}$.
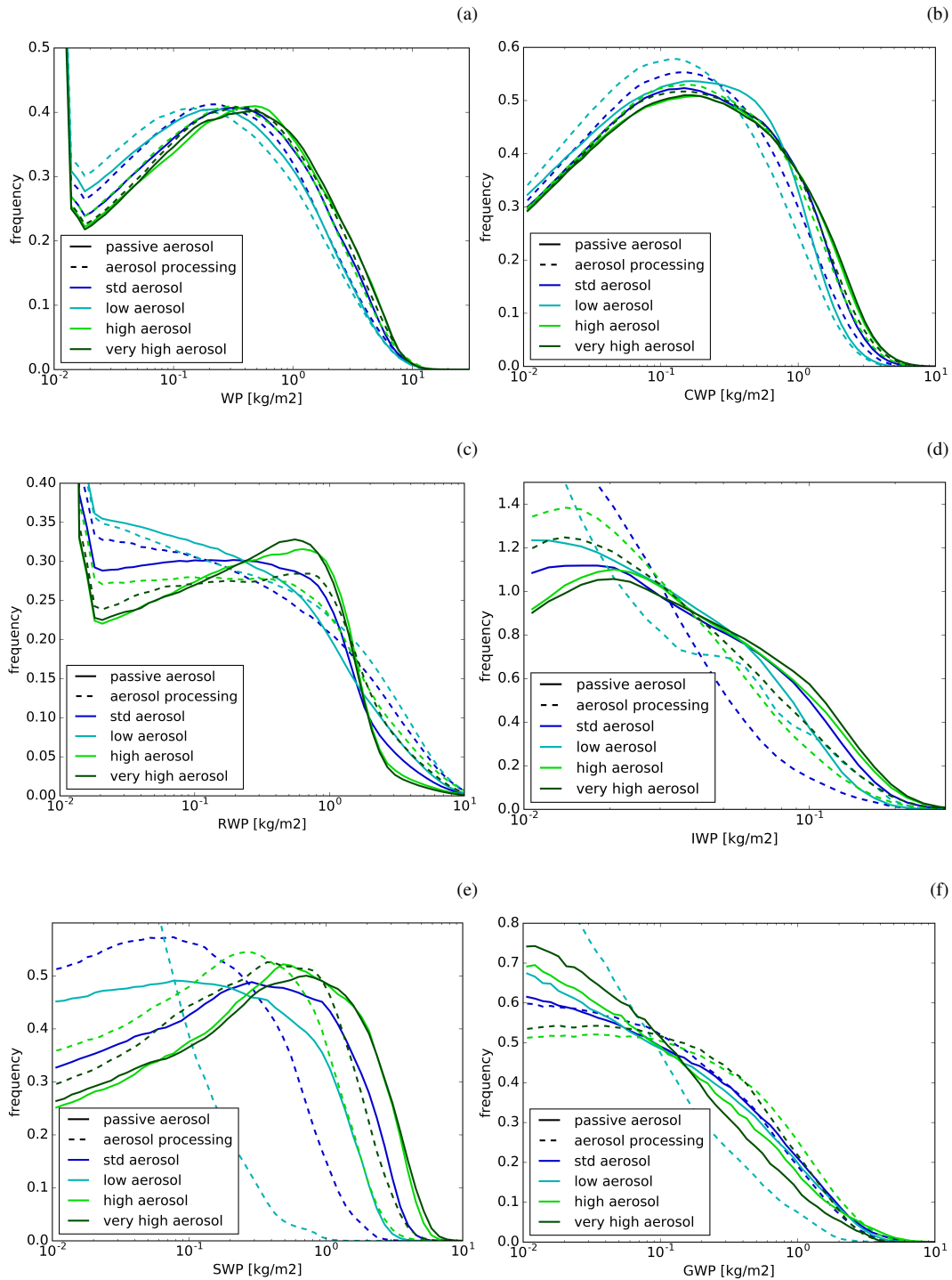
Figure 18. Frequency distributions of total condensed (a), cloud droplet (b), rain (c), ice (d), snow (e) and graupel (f) water path. Solid lines represent simulations with passive aerosols and dashed lines those with aerosol processing. Different line colours represent different aerosol scenarios.

19